Construction and Building Materials 414 (2024) 134811

Contents lists available at ScienceDirect

Construction and Building Materials

journal homepage: www.elsevier.com/locate/conbuildmat

Early age hydration behaviour of foam concrete containing a coal mining waste: novel experimental procedures and effects of capillary pressure

Esegbushota Josephine Foghi [a], Thanh Vo [a], Mohammad Rezania [a,*], Mohaddeseh Mousavi Nezhad [b], Liberato Ferrara [c]

[a] School of Engineering, University of Warwick, Coventry, United Kingdom
[b] Department of Civil and Environmental Engineering, School of Engineering, University of Liverpool, Liverpool, United Kingdom
[c] Department of Civil and Environmental Engineering, Politecnico di Milano, Milan, Italy

ARTICLE INFO

Keywords:
Cement hydration
Coal mining waste
Foam concrete
High capacity tensiometer
Matric suction

ABSTRACT

Globally, coal mining wastes (CMWs) are associated with significant environmental and economic costs. Processing CMW into an ingredient of foam concrete is a promising solution but the behaviour of this particular construction material has not been sufficiently evaluated, especially during the initial period of cement hydration. The purpose of this paper is to present novel laboratory set-up and experimental procedures designed to investigate the early age behaviour of hydrating foam concrete samples made with a CMW from Poland. Two types of tests were devised to simulate air-curing conditions and water-curing conditions, respectively. These tests were carried out in custom-built unsaturated oedometer cells, and the matric suction in the test samples was monitored for approximately 14 days, using Warwick high capacity tensiometers. Experimental results show that in both curing conditions, a higher matric suction during cement hydration corresponds to a denser sample at the end of the monitoring period. A comparison of water-cured and air-cured samples also reveals different responses to CMW inclusion in their mix designs. The responses can be convincingly explained based on complementary test data and idealised capillary tube models adapted for the hydrating foam concrete samples.

1. Introduction

Coal mining waste (CMW) is a by-product of mining and production of coal and it accounts for a significant share of coal production ranging from 10% to 15%, as a function of the variations in geological and mining conditions [1]. CMWs have been utilized successfully in many low to medium level civil engineering applications, such as controlled fills in mining zones, earthworks, and land restoration, as rock armor in shoreline structures, aggregates in road constructions and rail embankments [2]. However, the majority of CMWs have been so far dumped as cone-shaped heaps and tips, with the potential to cause environmental problems and become a constraint to economic developments in post-mining areas. The main effects of CMWs on the environment include dust pollution, air pollution from self-ignition, ground water contamination, visual impact, and potential slope failure of coal tips [2,3]. One way to lessen the environmental burden of CMWs is their reuse as a secondary raw material in construction, mostly in the production of concrete [4]. Concrete being the most widely used construction material, is still burdened with negative consequences resulting from the use of Portland cement, the production of which contributes significantly to global CO_2 emission [5]. Furthermore, the extraction of natural raw materials to be used as aggregates in concrete results in the depletion of natural resources. Therefore, the reuse of CMW in concrete mix design and production would reduce the use of cement binder as well as lower the dependence on natural raw materials to be used as primary aggregates [6].

However, the low strength and high carbon content of CMW as compared to natural aggregates, as well as the poor interfacial bonding with the cementitious matrix [7,8], limit the utilisation of CMWs as aggregates in high- performance concrete products [9,10]. Nevertheless, this limitation can be overcome in foam concrete, a lightweight cellular material mostly used for non- and semi-structural applications, where strength is not a parameter of primary consideration. In recent years, foam concrete has gained significant importance in the construction industry because of its unique properties including low density, high

Abbreviations: ASTM, American Society for Testing and Materials; CMW, Coal Mining Waste; FA, Foaming Agent; GSD, Grain Size Distribution; HCT, High Capacity Tensiometer; ID, Identification; RH, Relative Humidity; T, Temperature; SCM, Supplementary Cementitious Material.

* Corresponding author.
E-mail address: m.rezania@warwick.ac.uk (M. Rezania).

https://doi.org/10.1016/j.conbuildmat.2023.134811
Received 28 July 2023; Received in revised form 29 November 2023; Accepted 26 December 2023
Available online 13 January 2024

Nomenclature

α	pore water-pore solid contact angle
$A_{p\_optical}$	the number of pixels representing fraction of pore areas on a digital image
$A_{s\_optical}$	the number of pixels representing fraction of solid areas on a digital image
$A_{t\_optical}$	the number of pixels representing fractions of pore plus solid areas on a digital image
e_f	final void ratio
e_{filler}	void ratio of a filler material approximated from water absorption test
G_s, G_{s_avg}	specific gravity, average specific gravity
G_{s_CMW}	specific gravity of CMW
G_{s_cement}	specific gravity of cement
G_{s_sand}	specific gravity of sand
m_c	organic carbon content
m_{CMW}	mass of CMW
$m_{fillers}$	mass of filler material(s)
m_{FA}	mass of foaming agent
m_{foam}	mass of foam
m_{cement}	mass of cement
m_{sand}	mass of sand
m_w	mass of water
n_f	final porosity
R	radius of air-water interface curvature
r	radius of an idealised pore
ρ_{d_f}	final dry density
ρ_{w_f}	final wet density
s	matric suction
Sr	degree of saturation
T_s	surface tension of an air-water interface
u_a	pore air pressure
u_w	pore water pressure
V_a	volume of pore air
V_w	volume of pore water
w	gravimetric water content
w_{24hrs_filler}	water absorption.

flowability, controlled low strength, and excellent thermal, fire and acoustic insulation. As a result, it has been used in many applications, including insulation and fire protection, utilising its high thermal insulation capacity, geotechnical highways, bridge abutments and filling applications [11–13]. A similar concept, named "collapsible" concrete, based on low binding of gap-graded lightweight aggregates by means of an air entrained cement paste with high water/cement ratio has also been proposed for sacrificial protection against accidental events, including blasts and explosions [14,15].

Fly ash, an industrial by-product of coal production, has been extensively used as lone supplementary cementitious material (SCM) [5] or combined with other additives in Portland cement-based concrete to deliver mechanical performance superior to the control concrete [16]. In fact, wastes and by-products from a variety of sources, such as rice husk ash, expanded perlite aggregate, glass fines, waste seashells, silica fumes, blast furnace slag, and fly ash [17–22] have been utilised as raw materials in the production of aerated and foam concrete. Despite the many reports of CMWs being successfully processed into SCM, the use of CMWs in the construction industry as raw material is limited [2]. Researchers have shown that some aerated and foam concrete mixes containing CMWs as raw material can, through tailored curing, develop mechanical performances comparable to their counterparts not containing CMWs [20,23,24].

With respect to curing condition, better mechanical resistance has been reported for foam concrete samples after 28 days of curing in water (or at a relative humidity (RH) $\approx$ 100%) compared to those cured in air at natural RH ($<<$ 100%) and laboratory temperatures (20 °C $\pm$ 5 °C) [25–27], as it was suggested that optimal moisture levels for cement hydration may not be reached in air-curing environments.

Uning emission scanning electron microscopy micrographs, Falliano et al. [28] observed significant differences in pore morphology (and mechanical behaviour) between foam concrete specimens after 28 days of curing in air and in water. Small and diffused microcracks were more abundant in air-cured samples. In this respect, while most previous experimental studies have tested foam concretes after they have hardened sufficiently to permit handling and mechanical testing, the properties of foam concretes in their "fresh" in situ state have been comparatively much less explored. Research studies published recently [29–31] point to fresh state properties as early indicators of hardened state properties.

Jamali et al., [32] have recently used high capacity tensiometer (HCT) to capture real time capillary pressure (matric suction hereafter) in early age concrete specimens, to develop a four-stage hydration model, where the rate of matric suction evolution was found to be indicative of water evaporation, self-desiccation, setting time, temperature, and hydration processes. The overall porosity of concrete specimens was not reported however scanning electron microscope was used for observation of concrete specimens' pore size distribution (down to 0.7 μm). HCT was reportedly used for the first time in that study to investigate early age concrete behaviours. HCTs have been the key behind many recent advancements in experimental unsaturated geomechanics. They are typically used in unsaturated soil laboratories to directly measure matric suctions greater than 100 kPa, generating significant interest for their accuracy and fast response time [33,34]. It is the authors' knowledge that HCT has not yet been applied to foam concrete research, or to understand the variations in cement hydration kinetics and mechanisms that can occur in concrete containing different kinds of recycled constituents, least of all recycled CMWs.

Therefore, the objective of this study is to investigate the fresh state properties of foam concrete and their evolution into hardened state properties using a novel set of experimental equipment and procedures. In particular, this article explains (1) how a foam making device can be developed from readily available laboratory components, and how foam characterisation can be carried out to determine an optimal dilution ratio and compressed air pressure to produce stable foam for concrete-making; (2) how HCTs can be incorporated into two custom-made cylindrical cells, and how the system can be configured to simulate the distinct hydration conditions (water-curing and air-curing) to determine the impacts of different curing environments on the early age behaviour of the foam concrete samples; (3) how matric suction, measured by the HCTs during the cement hydration in different drying environments, can be interpreted in a simple way via an idealised theoretical model, and how the measurement may serve as a real-time indicator of foam concrete hydration progress; and finally, (4) how utilising CMWs to partially replace fine aggregates (sand) in a foam concrete recipe may affect its final density (after hardening).

2. Materials

Waste and by-products of diverse sources have been used in foam concrete as either a partial or total replacement of cement and fine aggregates, to reduce the energy consumption and CO_2 emissions related to cement production, conserve the natural resources and protect the environment. Wastes with a certain degree of pozzolanic reactivity and adequate fineness such as fly ash and bottom ash, as well as those with high amorphous silica content e.g., rice husk ash, seashell, waste glass

and silica fume, have been used as supplementary cementitious materials [17–19,35,36]. On the other hand, wastes available in larger sizes and with low pozzolanic reactivities such as mining wastes, construction and demolition wastes are primarily used as replacements for fine aggregates. The waste material investigated in this study is a CMW, used as a partial replacement for the natural sand in foam concrete making.

The porous structure of foam concrete is attained by introducing aqueous foam into cement paste or mortar. Foams are created using different types of foaming agents (FA), e.g., protein-based foaming agents, synthetic foaming agents. In this study, a protein-based foaming agent has been used. Protein-based foaming agents can produce small isolated spherical air bubbles resulting in a strong and closely spaced stable cellular structure as well as a foam concrete product with reasonably high compressive strength [18,36]. Foaming agents are typically used in conjunction with other organic and inorganic additives to control various mix properties. However, no additives were used in this study, limiting the composition to only 5 foam concrete ingredients (Fig. 1) in order to provide a clearer picture of the constituents' effects. It is worth mentioning that the foam was created in the laboratory according to a calibrated procedure to ensure consistent properties when poured into the fresh mixtures.

2.1. Concrete constituents

Cement CEM II/A-LL 32.5 R supplied by Hanson UK (with main particle size 5–30 mm, and 86% of grains (by weight) being finer than 0.063 mm) and silica sand (55% SiO_2 as determined from X-ray fluorescence) were used as main ingredients to produce the foam concrete samples. The grain size distribution (GSD) of the sand used in the foam concrete mixes is shown in Fig. 2. The CMW which was used as a partial replacement of the natural silica sand is an aggregate sourced from Piast coal mine in Bieruń, Poland. It was taken from a jig separator at the mine, crushed into smaller particles inside a cylindrical chamber of 145 mm diameter using a 1000 kN actuator (Servocon Systems Ltd, UK), then sorted into different sizes; those particles that were finer than 2.36 mm were used to make foam concrete (as partial replacement for the sand). Fig. 2 shows the GSD of this CMW pre-sorting, i.e., as obtained from the rig separator, and post-sorting, i.e., as used in the foam concrete paste preparation of cylindrical specimen with a diameter of 75 mm and a height of 28 mm. The maximum particle size of this CMW was selected to be 2.36 mm to achieve similarity with the particle size of the sand for a uniform blend. The specific gravity (G_s), water absorption ($w_{24hrs\_aggregate}$) and organic carbon content of the aggregates used to make the foam concrete are listed in Table 1.

Sand and Piast CMW can themselves be considered as porous geomaterials. Taking the degree of saturation $Sr = 1$ for the aggregate material post- 24 h soaking in a water absorption test, an aggregate void ratio ($e_{aggregate}$) can be calculated as $e_{aggregate} = w_{24hrs\_aggregate} \times G_s$. An aggregate porosity ($n_{aggregate}$) can be calculated as $n_{aggregate}=e_{aggregate}/(1+e_{aggregate})$. The water absorption test described in BS 20290–1 [37] was followed in this study. Table 1 shows that $e_{aggregate}$ is much higher for Piast post-sorting than for sand (0.12 compared to 0.034), indicating that the CMW is much more porous than the natural sand. A water cement ratio equal to 0.4 was adopted in the mix designs to investigate the impact of different water absorption capacities of the employed natural and CMW aggregates on the matric suction s measured in the pore spaces during cement hydration and the resultant concrete porosity. The adopted mix designs are detailed in Table 2.

As evident in Table 2, for simplicity, the mass of cement, the total mass of aggregates ($m_{aggregates}$), the mass of water and the mass of foam (m_{foam}) were kept constant, while the mass of sand (m_{sand}) and the mass of Piast CMW (m_{CMW}) were changed to assess the impacts of replacing different percentages of sand with CMW.

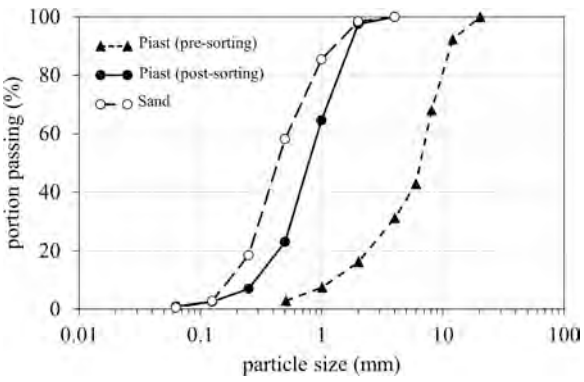

Fig. 2. Grain size distributions of Piast CMW from Bieruń, Poland (pre- and post-sorting) and of a sand used in the foam concrete mixes.

Table 1
Index properties of the aggregates.

	Piast CMW (post-sorted)	Sand
G_s	2.56	2.62
$w_{24hrs\_aggregate}$	4.7%	1.3%
$e_{aggregate}$	0.12	0.034
$n_{aggregate}$	0.11	0.033
organic carbon content	8.84%	0%

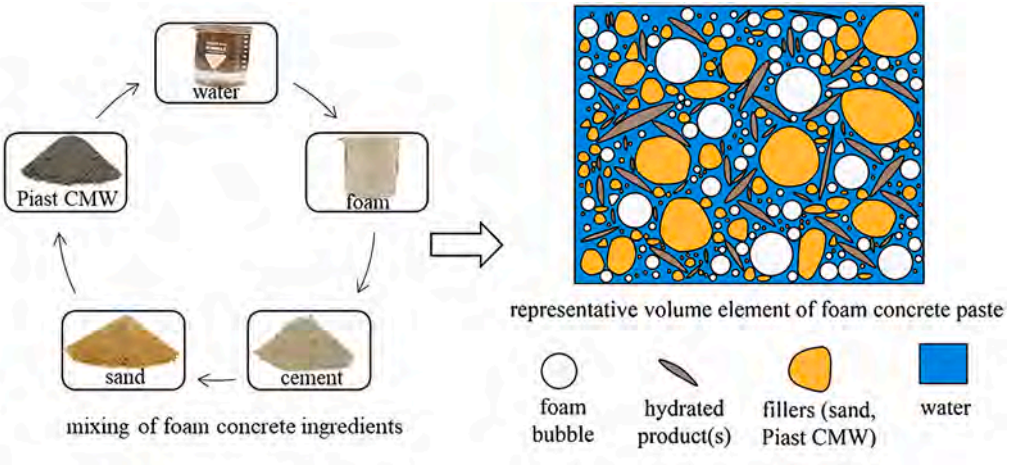

Fig. 1. Ingredients employed to produce foam concrete.

Table 2
Details of the mixture proportions per cubic meter.

Mix ID	M1	M2	M3	M4
Cement (kg)	333.3	333.3	333.3	333.3
Sand (kg)	333.3	299.97	266.64	233.31
CMW (kg)	0	33.33	66.66	99.99
Water (kg)	133.3	133.3	133.3	133.3
Foam (kg)	31.77	31.77	31.77	31.77
w/c	0.4	0.4	0.4	0.4

2.2. Foaming agent

The structure of foam and its distribution in a setting paste are indicative of properties achieved by the hardened foam concrete [38]. Different foam production methods have been reported in the literature, including chemical foaming, air entrainment, and mixing with aqueous precursor foam (also referred to as the pre-forming method) [11,39]. In the latter, cement slurry and aqueous foams are prepared separately before being mixed. The pre-forming method has been adopted in this study as it was reported to require lower foaming agent and result in a close relationship between the amount of foaming agent used and the air content of the mix [13]. It was also found that this method facilitates larger and more accurate foam entry compared to the mixed foaming method [40]. A protein-based foaming agent (Propump 26 supplied by Propump Engineering Ltd, UK) was used in this study, featuring a density of 1.12 (g/mL) and pH of 6.5–7.5.

3. Equipment set-ups and test procedures

3.1. A foam generation device

A foam generation device was custom-built in the laboratory using standard laboratory components. A schematic view of the device is shown in Fig. 3. It permits air with pressure between 0 and 450 kPa to be introduced into an enclosed cylinder (of 1338 cm^3 in volume) and turbulently mixed with a targeted amount of diluted foaming agent. The mixing of the two phases generates the foam.

3.2. Foam characterisation

Measurements of foaming capacity and stability were conducted previously [38] to assess how a foaming agent entrains air in concrete. In this study, the effectiveness of the produced and employed foam [39] was assessed by examining the density and stability of the foam produced at different foam generation pressures (150, 200, 250, 300, 350, 400 and 450 kPa) and foaming agent (FA) concentrations (m_{FA}/m_w=2%, 4%, 6%, 8% and 10% where m_{FA} and m_w denote the mass of foaming agent and the mass of water, respectively).

Immediately after foam production, the foam density was measured by filling a pre-weighed standard container of known volume with the foam and weighing it. The foam stability was evaluated by measuring the mass of liquid that drained from the bottom of the foam at 5, 10, 30, 60, 120, 180, 240 and 360 min.

The effects of FA concentration and foam generation pressure on the foam density are shown in Fig. 4a. For a foam generation pressure between 150 kPa and 450 kPa, it is shown that an increased FA concentration corresponds to a decreased foam density. Fig. 4a also shows that the foam generation pressures have minor impact on the foam density. As the targeted foam density was 50 ± 5 kg/m^3 in this study, a FA concentration of 8% and a foam generation pressure of 350 kPa were adopted to create the foam for the concrete mixes.

Fig. 4b shows the drainage of foam (% mass changed from gas phase

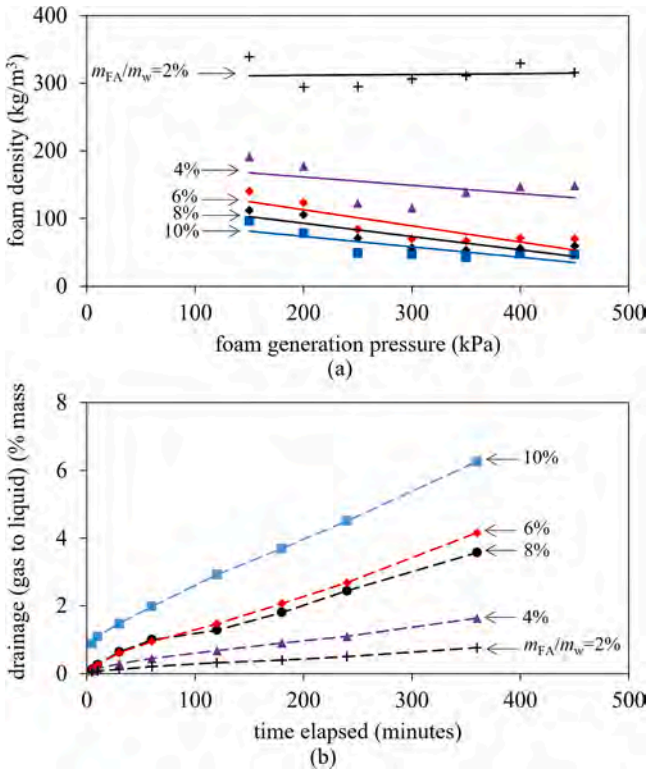

Fig. 4. (a) Impacts of air pressure and foaming agent (FA) concentration on foam density and (b) effect of FA concentration and elapsed time on foam drainage.

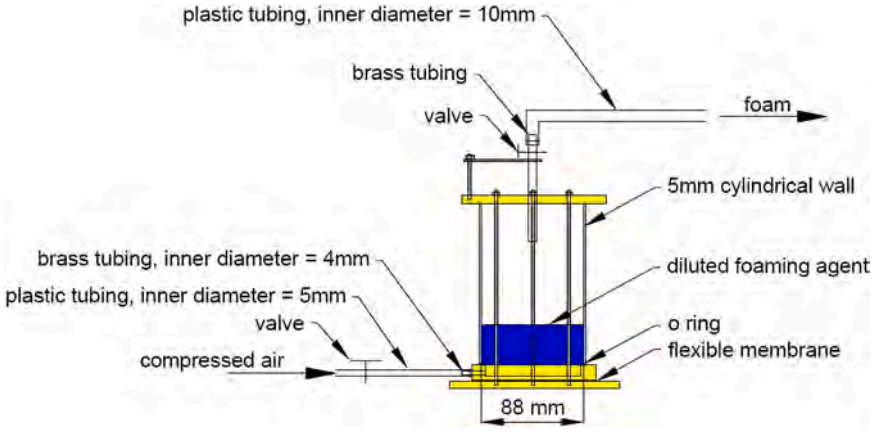

Fig. 3. Schematic diagram of the foam generation device.

to liquid phase) created at different FA concentrations and at a foam generation pressure of 350 kPa as a function of the time elapsed since the completion of the test container filling. An increase in FA concentration corresponds to an increase in the drainage i.e., the foam created at a higher FA concentration was less stable. However, at the selected FA concentration in this study (m_{FA}/m_w=8%), after 6 h (360 min), only less than 5% of the foam mass changed from a gaseous phase to a liquid phase. It will be shown in the sequel (Section 4) that the foam concrete mixes hydrated rapidly, mostly within the first 2–24 h after mixing.

3.3. Instruments, set-ups, and procedures to monitor hydration of foam concrete

The hydrating foam concrete considered in this study contained significant volumes of air and water (in addition to the solid fraction) so it is described using unsaturated geomechanics terminologies. Researchers have systematically classified pores of aerated and foam concretes [38]. Except if stated otherwise, the term "pore" in this paper refers to the volume other than the solid fraction (= aggregate particles + unhydrated/hydrated products) in a sample. In an unsaturated geomaterial, the evacuation of capillary water from the pore space changes the matric suction ($s = u_a - u_w$) there, where u_a and u_w are pore air pressure and pore water pressure, respectively. This change in the matric suction s can be measured directly by a tensiometer. In recent years, there has been significant interet in the use of high capacity tensiometers (HCTs) in unsaturated soil mechanic laboratories to measure matric suctions > 100 kPa, due to their accuracy and fast response time. Details of the custom-built HCTs used in this study have been reported previously for direct and long-term measurement of suction in fine-grained geomaterials [33,34,41,42]. Fig. 5 shows a schematic view (Fig. 5a) and an annotated photograph (Fig. 5b) of the Warwick HCT. What distinguishes these HCTs are the surface-polishing techniques employed to reduce the surface roughness of the HCTs' diaphragms in order to minimize the presence of gas nuclei in their water reservoirs [41,42]. This allows for an enhanced cavitation threshold and hence improved maximum attainable suction and maximum measurement duration. Each HCT consists of a 0.4 mm thick × 7 mm diameter internal diaphragm, a water reservoir of 0.1 mm deep × 6 mm diameter and is fitted with a 1.5 MPa air entry value ceramic disc.

The experimental set-up includes two unsaturated oedometer cells

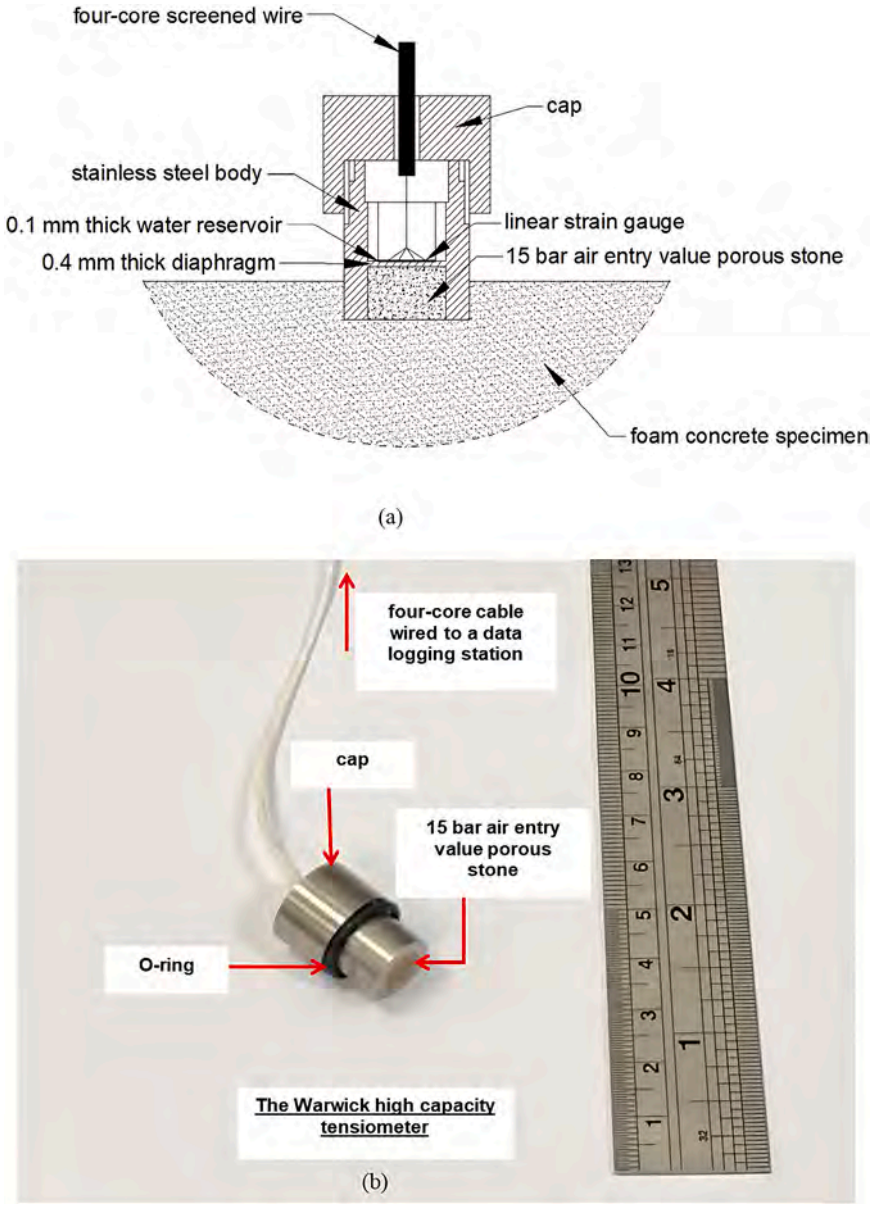

Fig. 5. (a) A schematic view and (b) an annotated photograph of the Warwick HCT.

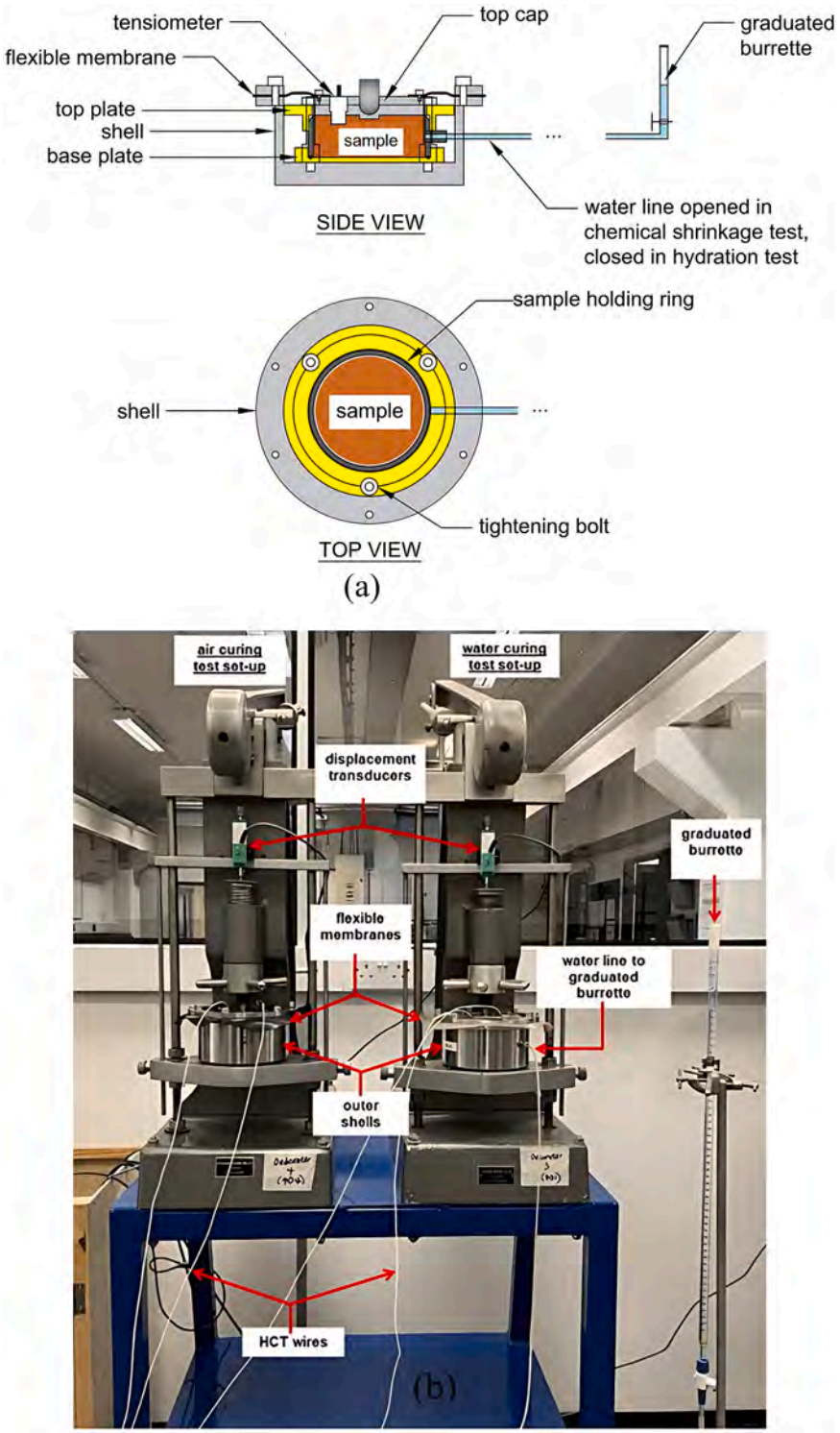

Fig. 6. (a) A schematic view and (b) an annotated photograph of the custom-built unsaturated cells to monitor hydrating foam concrete.

(Fig. 6a) custom-built for the characterisation of unsaturated geomaterials. Each cell (Fig. 6a) accommodates a cylindrical specimen of 75 mm diameter and 28 mm height placed inside a steel ring and supported on a brass plate. The top cap is fitted with a HCT that to be brought into direct contact with the specimen to measure the matric suction along the contact points. In the experiments carried out in this work, the HCTs were pushed 5–6 mm into the samples to maintain good contact. As the total volume of a sample is approximately 39.4 cm^3 only, this matric suction is taken to be the prevailing value in the sample. A flexible membrane was used to prevent moisture exchange between the sample surface and the external environment, as shown in Fig. 6a.

Two oedometer cells were used in this study to conduct two types of tests, namely, air-curing test and water-curing test.

The air-curing test set-up is a closed system, in which the sample is air-cured while being sealed from the external environment. The water-curing test set-up is an open system, while analogous to the first set-up in most details, it was modified to accommodate a water line connected to an external graduated burette (Fig. 6). This is to monitor the amount of

water absorbed by the specimen while the same is consumed by hydration reactions. The water-curing cell is similar to the ASTM dilatometry test set-up [43] for determining the chemical shrinkage of hydraulic cement paste. Prior to the experiments, a null test was carried out to determine the lowest water level in the burette that kick-starts a flow into the cell. In particular, the water line was opened to allow for water to flow into the empty cell (without a sample), and the point on the burette when the water flow stopped, was noted as the initial water level. For the set-up in this study, this point was located approximately 30 mm above the sample surface.

As the effect of applied load on the hydration behaviour of the samples was not the concern of this study, the air-curing and water-curing tests were performed without targeted loading of the oedometer cells. However, a small vertical stress was applied to the specimens by the loading cap, and this was accounted for in the initial height of the specimen. The experiments were conducted in a laboratory environment where, over the testing period, temperature, and relative humidity (RH) were measured to be 22–25 °C and 30–50%, respectively.

In a recently published study [32], HCTs have been used to monitor the early age behaviour of concrete, however to the authors' knowledge, they have never been applied to study the behaviour of hydrating foam concrete. The response of HCTs to matric suction depends on how well their tips, including both the high air entry ceramic disc and the water reservoir behind the disc, are saturated. In this study, HCTs were saturated in a custom-built saturation chamber [34] following a procedure similar to [33]. Prior to being placed into contact with a test specimen, the HCTs were saturated and preconditioned following the procedure explained by [33]. The tip of each HCT was covered with a thin layer of fresh foam concrete mix to ensure ultimate contact between the specimen and the HCTs. The HCTs were connected to the data logger system and suction values were recorded at 5-minute intervals.

3.4. Digital imaging set-up and analysis

Analysis of digital images (from digital camera, scanning electron microscopy, X-ray micro-computed tomography) has been successfully used by researchers to investigate microstructural features of foam concretes [44–46]. In this study, digital image analysis is used to identify porous features of hydrating foam concrete samples to complement visual observation and aid the interpretation of water-curing and air-curing test data.

Equipment set-up is relatively simple. The footprints of 4 sample rings (of identical dimension to those used in the unsaturated oedometer cells) were milled onto the surface of a steel plate. A rubber O-ring sits inside the groove beneath each ring while it is loaded with a small vertical pressure to prevent the leaking of fluid from inside the ring to the exterior. After pouring, the surface of each sample was carefully levelled and trimmed to just below the top edge of the ring. A transparent plastic plate (with a small weight on top of it) is placed over the samples to limit air-drying from exposure to the environment. At specific time intervals after pouring (i.e., at the 0, 30, 60 min and then at 2, 4, 24, 48, 72 h and 10 days) the plate is lifted off for photography; thus, the curing condition of these 4 samples is not exactly the same as that of the air-curing tests detailed in Section 3.3. A Nikon Z6 DSLR camera was

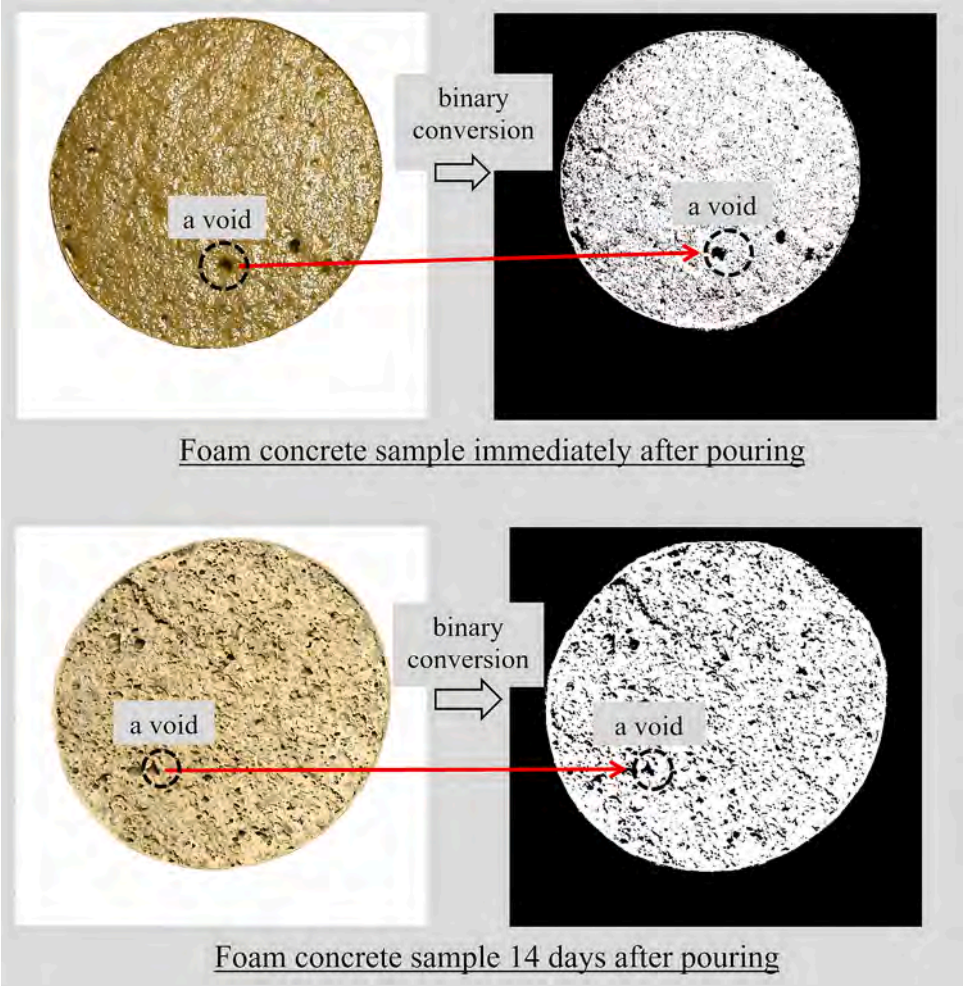

Fig. 7. Digital image analysis procedure.

used for taking photographs of the samples. The lens of the camera (NIKKOR Z 24–70 mm 1:4 S ϕ72) was set at 1 m from the surface of the samples, and its optical axis approximately orthogonal to the surface of the steel plate. The camera was supported on a tripod and the remote shooting function was used. When an image was taken, background lighting was turned off and direct lighting was provided by a fluorescent lamp.

The images, acquired as above, were converted into binary format (where black represents the pore fraction and white represents the solid fraction) as shown in Fig. 7. A ratio of the pore fraction to the solid fraction can be approximated from:

$$\frac{A_{p\_optical}}{A_{s\_optical}} = \frac{A_{t\_optical} - A_{s\_optical}}{A_{s\_optical}} \tag{1}$$

where $A_{p\_optical}$, $A_{s\_optical}$, $A_{t\_optical}$ are the number of pixels used to represent the pore fraction, the solid fraction and the sum of pore and solid fractions of a sample on an image, respectively. The ratio in Eq. 1 is not the same quantity as the void ratio (e) of a sample because this ratio is calculated from a two-dimensional (2D) image. A 2D image cannot account for the tortuosity of the pore network in the third direction perpendicular to the camera lens, it also does not account for the pore space within the aggregates/hydrated products making the solid fraction, and it requires a subjective assessment of a greyscale to binary conversion threshold to distinguish between pore water and pore air. Nevertheless, when ambient lighting and camera setting are constant throughout a test, the ratio in Eq. 1 can be used to identify quantitatively major developments of the pore fraction in a hydrating foam concrete sample.

The binary conversion was automated in MATLAB version R2018b. For each photograph taken on each sample during the 20,160 min (=14 days) monitoring period, a calibration was carried out to determine a suitable greyscale to binary conversion threshold. To do this, the pores observed on a coloured photograph were visually matched against their corresponding representations on a binary image to obtain a suitable threshold (Fig. 7).

3.5. Specimen preparation

Cement paste and foam were prepared separately to produce a foam concrete sample. To obtain the cement paste, selected geomaterials (sand and/or Piast CMW) were oven-dried at 105 °C, cooled down to laboratory temperature then combined with cement in a mixer for half a minute. Thereafter, the required quantity of water was added, and mixed further for approximately 4 min. To obtain the foam, the protein-based FA was diluted to a concentration ratio (i.e., m_{FA}/m_w) of 8% inside the foam generator (Fig. 3). Then, compressed air at 350 kPa was introduced into the generator to turbulently mix with the surfactant solution to produce the targeted foam. Subsequently, the required amounts of foam and cement paste were blended and slowly stirred for up to 1 min to obtain a homogeneous state (Fig. 8). To cast a foam concrete specimen, the mixture was slowly poured into a sample holding ring in a circular motion until the ring was full. Then, the sample was carefully levelled and trimmed to just below the top edge of the ring (Fig. 8).

4. Test results

A test program was conducted to investigate the water absorption property and the pore structure development of early age foam concrete samples made with Piast CMW, by way of the water-curing test and the air-curing test, both described in Section 3.3, and the digital image analysis described in Section 3.4.

At the end of each test, after approximately 14 days, e_f was calculated from the mass and volume of the oven-dried sample according to:

$$e_f = \frac{G_{s\_avg}(1 + w_f)}{\rho_{w\_f}} - 1 \tag{2}$$

where w_f, and ρ_{w_f} denote the final gravimetric water content and the final wet density of the sample, respectively. G_{s_avg} is the specific gravity of the solid fraction in a foam concrete sample and is approximated from the following equation:

$$G_{s\_avg} = \frac{G_{s\_CMW} \times m_{CMW}}{m_{CMW} + m_{cement} + m_{sand}} + \frac{G_{s\_cement} \times m_{cement}}{m_{CMW} + m_{cement} + m_{sand}} + \frac{G_{s\_sand} \times m_{sand}}{m_{CMW} + m_{cement} + m_{sand}} \tag{3}$$

where G_{s_CMW}, G_{s_cement}, and G_{s_sand} denote the specific gravity of Piast CMW, cement and sand, respectively. e_f, w_f, $n_f = e_f/(1 + e_f)$ of samples in this test program are listed in Table 3.

4.1. Water-curing test results

Fig. 9 shows the rate of water consumption of the foam concrete mixes M1, M2, M3 and M4 over the 14 days monitoring period. The

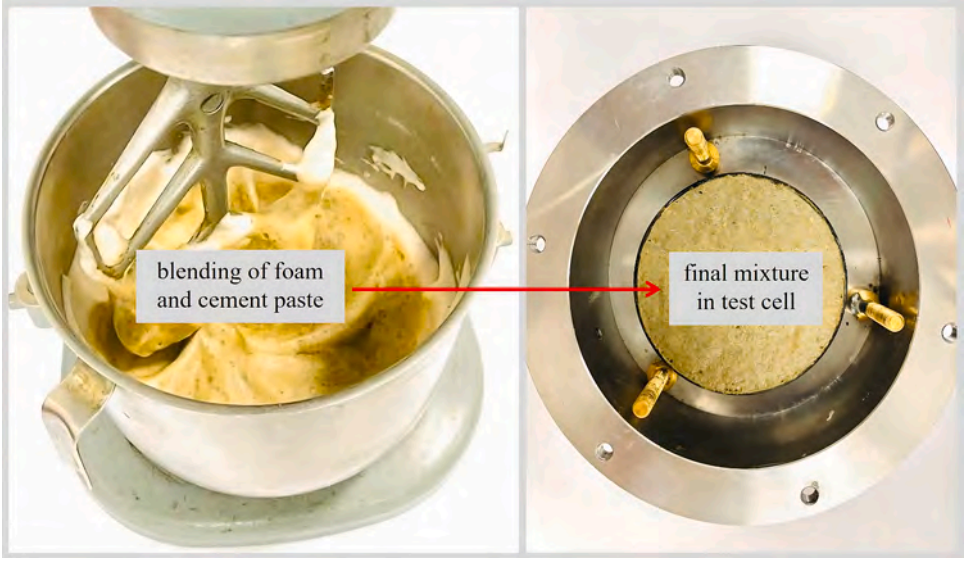

Fig. 8. Foam concrete specimen preparation.

Table 3
Details of test samples.

Mix ID	M1	M2	M3	M4
e_f of water-curing sample	1.73	1.73	2.26	2.23
w_f of water-curing sample	0.18	0.19	0.27	0.29
n_f of water-curing sample	0.63	0.63	0.69	0.69
e_f of air-curing sample	2.46	2.22	1.96	1.69
w_f of air-curing sample	0.074	0.134	0.162	0.164
n_f of air-curing sample	0.71	0.69	0.66	0.63
e_f of digital imaging analysis sample	2.4	2.05	1.93	1.72
w_f of digital imaging analysis sample	0.06	0.07	0.08	0.09
n_f of digital imaging analysis sample	0.70	0.67	0.66	0.63

rapid rises in water consumption in early age results (<24 h) are comparable to those reported by [47] for similar cement types and curing conditions (although it should be noted that Bouasker et al.'s (2008) paste did not contain any foam). As the percentage of sand replaced by Piast CMW (i.e., $m_{CMW}/m_{fillers}$ ratio) increases, more water is consumed during the cement hydration. The chemical shrinkage coefficient of mix M1 (containing no CMW) is approximately 0.032 mL/g of cement (CEM II/A-LL 32.5 R) after 24 h, and 0.06 mL/g at the end of day 14. As shown in Fig. 9, these values are notably smaller than the chemical shrinkage coefficients of mixes M2, M3 and M4 which contain Piast CMW (these coefficients of mixes M2, M3, M4 are 0.07 mL/g, 0.157 mL/g, 0.159 mL/g, respectively, after 24 h, and are 0.146 mL/g, 0.282 mL/g, 0.351 mL/g, respectively, at the end of day 14). This is not surprising given that the Piast CMW geomaterials incorporated into the M2, M3, and M4 mixes were much more porous than the sand particles they replaced (Table 1). Also shown in Fig. 9 are water consumption plots (dashed lines) for $WA_{24hours\_sand+CMW} = 0\%$ i.e., assuming that sand and CMW in the mixes did not absorb any water. They show that higher water volumes lost during hydration in mixes with higher percentages of Piast CMW are minorly due to different amounts of water absorbed by the porous aggregates, in fact, other contributing factors such as different grain size distributions (thus pore size distributions, particle/pore morphologies) and different mineralogies between sand and Piast CMW may have played a more significant role. The vertical axis in Fig. 9 was plotted in logarithmic scale to clearly show that water volume measurements did not change at the start of monitoring, but after 1 to 5 h from the start of monitoring, they increased rapidly (from approximately zero) then flattened out according to typical chemical shrinkage results of OPC concrete. The presence of foam bubbles in the specimens may have initially prevented continuous flows of water to occur until matric suctions have developed sufficiently (first in mixes M1 and M3 after more than 1 h, then in mixes M2 and M4 after more than 4 h from the start of monitoring) to draw in external water for continued hydration.

Fig. 10 shows matric suctions measured by the HCT in water-curing tests of the foam concrete mixes M1, M2, M3, M4. The suctions rose sharply during the first 24 h then stabilised and/or slowly decreased over time. After 1 h from the start of monitoring, the matric suctions had risen higher (and subsequently stabilised earlier) in mixes M1 and M3 compared to mixes M2 and M4. The small fluctuations observed in the suction plots are related to periodic variations in the ambient condition. Fig. 10 shows that higher maximum matric suctions were registered in those samples with lower percentages of Piast CMW (i.e. the highest in mix M1 ($m_{CMW}/m_{fillers}$=0), second highest in mix M2 ($m_{CMW}/m_{fillers}$=0.1), second lowest in mix M3 ($m_{CMW}/m_{fillers}$=0.2), and the lowest in mix M4 ($m_{CMW}/m_{fillers}$=0.3)). In these water-curing tests, it was found that at the end of the monitoring period, samples with lower percentages of Piast CMW generally had lower final moisture contents w_f and lower final void ratios e_f. This observation will be compared with the results from air-curing tests and image analysis findings, in the following sections.

It should be noted that already at the start of monitoring, the samples were not fully saturated due to the presence of stable foam (m_{foam}/m_{cement}=0.11) in their formation.

4.2. Air-curing test results

Fig. 11 shows the matric suctions measured by the HCT of the foam concrete mixes M1, M2, M3, M4 during the monitoring period. The suctions rose sharply in mixes M1, M3, and M4 during the first 1–2 days, then stabilised for a period of between 1–3 days before rising sharply again to the HCT cavitation values. For a given mix (as summarised in Table 2), the maximum suction registered was much higher in the air-curing test than in the water-curing test e.g., for mix M3, a maximum suction of 2092 kPa was measured in the air-curing test compared to 359 kPa in the water-curing test.

It can be observed in Fig. 11 that during much of the increase to HCT cavitation values, suction values were higher in samples with higher percentages of Piast CMW (i.e. the highest in mix M4 ($m_{CMW}/m_{fillers}$=0.3), second highest in mix M3 ($m_{CMW}/m_{fillers}$=0.2), second lowest in mix M2 ($m_{CMW}/m_{fillers}$=0.1), and the lowest in mix M1 ($m_{CMW}/m_{fillers}$=0)). At the end of testing, air-cured samples with higher percentages of Piast CMW were measured to have lower final void ratios e_f and higher final moisture content w_f values.

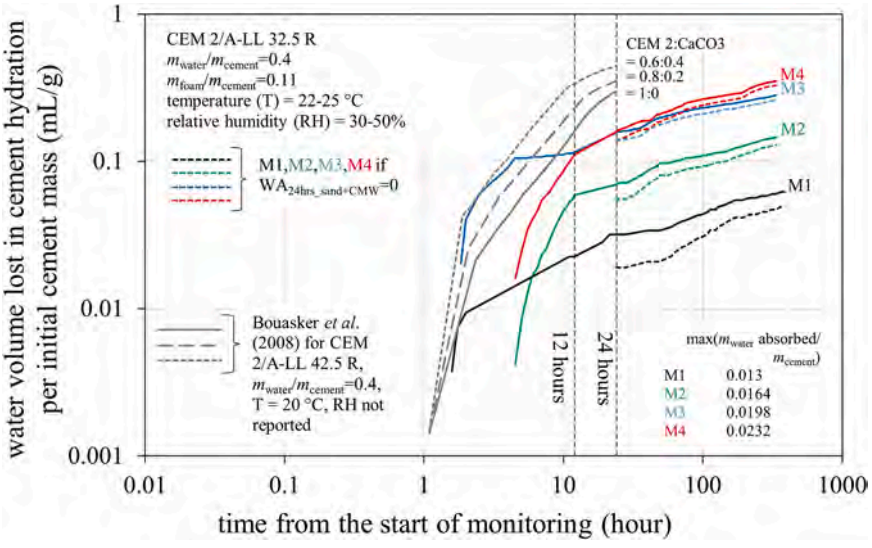

Fig. 9. Water-curing test results in terms of the water consumption.

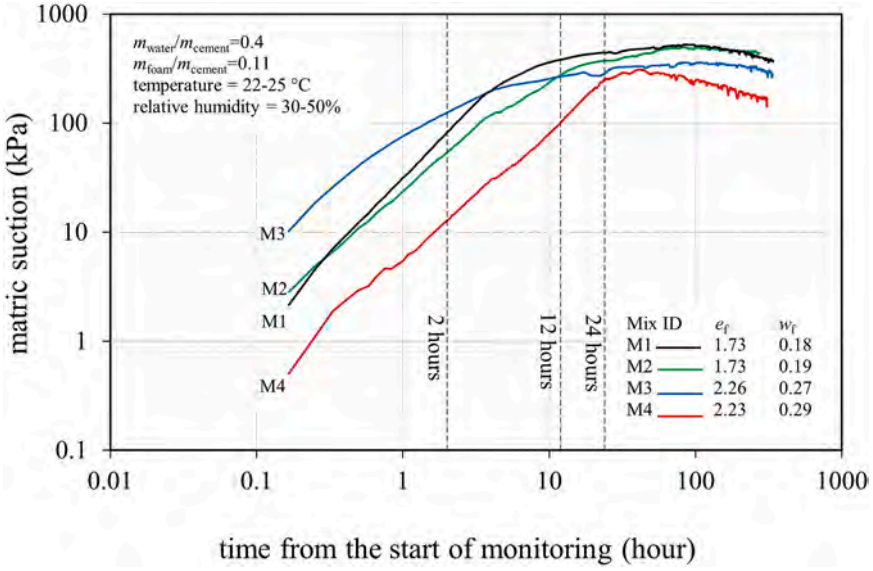

Fig. 10. Water-curing test results in terms of the matric suction evolution.

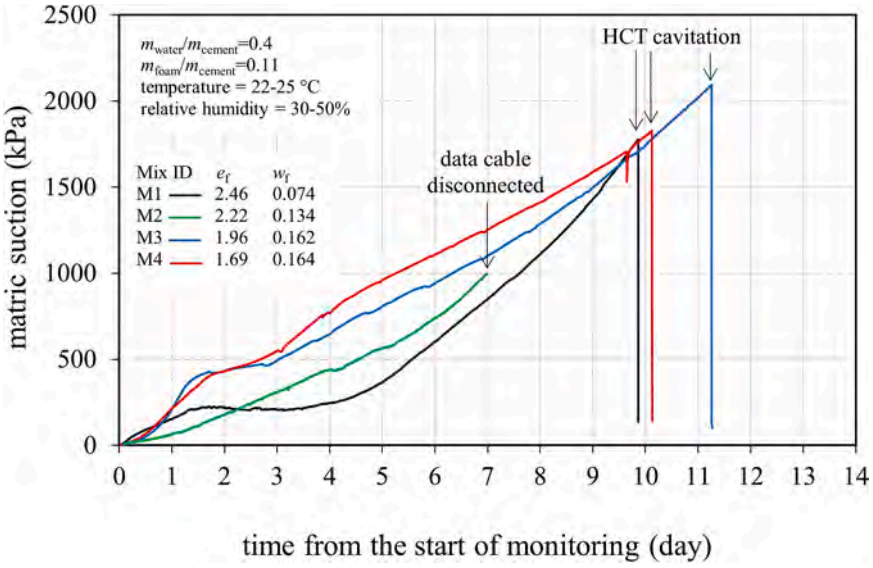

Fig. 11. Air-curing test results in terms of the matric suction evolution.

Thus, in both air-curing and water-curing tests, higher suctions registered by the HCT generally corresponded to samples having higher final dry density ρ_{d_f}. However, for the mixes adopted here, samples with higher percentages of Piast CMW may result in lower ρ_{d_f} in the water-curing test but higher ρ_{d_f} in the air-curing test (a possible mechanism underlying these measurements is discussed in Section 4.4).

4.3. Digital imaging analysis

Fig. 12 shows the pore to solid areas ratio ($A_{p\_optical}/A_{s\_optical}$) obtained by the digital imaging technique. The inherent limitations of the adopted 2D optical method (as detailed in Section 3.4) cause apparent scattering in the plots for mixes M1, M2, M3, M4; nevertheless, it is clear that $A_{p\_optical}/A_{s\_optical}$ changed rapidly after pouring but became stable after a few hours, and this is consistent with visual observations of these samples in the laboratory.

Of interest are the final void ratios e_f and final moisture contents w_f included in Fig. 12 and Table 3. The digital imaging samples with higher percentages of Piast CMW have higher final dry density ρ_{d_f} and higher final moisture content w_f, similar to the observation made on the air-curing test results (Section 4.2). It was also mentioned in Section 3.4 that the boundary condition of paste mixes M1, M2, M3, M4 studied in digital imaging was closed for most of the monitoring period except when their covering plate was lifted off for taking photos and measurements, possibly causing their final moisture contents to be smaller than those of their analogous samples in the air-curing tests (Fig. 12 compared to Fig. 11, also listed in Table 3).

4.4. Capillary models for hydrating foam concrete samples

Idealised capillary tube models for air-curing and water-curing test samples are shown Fig. 13. Air, water and solid materials are assumed present at the pore scale. Pressure difference across the pore air-water interface may be approximated by Young-Laplace's equation:

$$u_a - u_w = s = \frac{2T_s}{R} = \frac{2T_s\cos\alpha}{r} \quad (4)$$

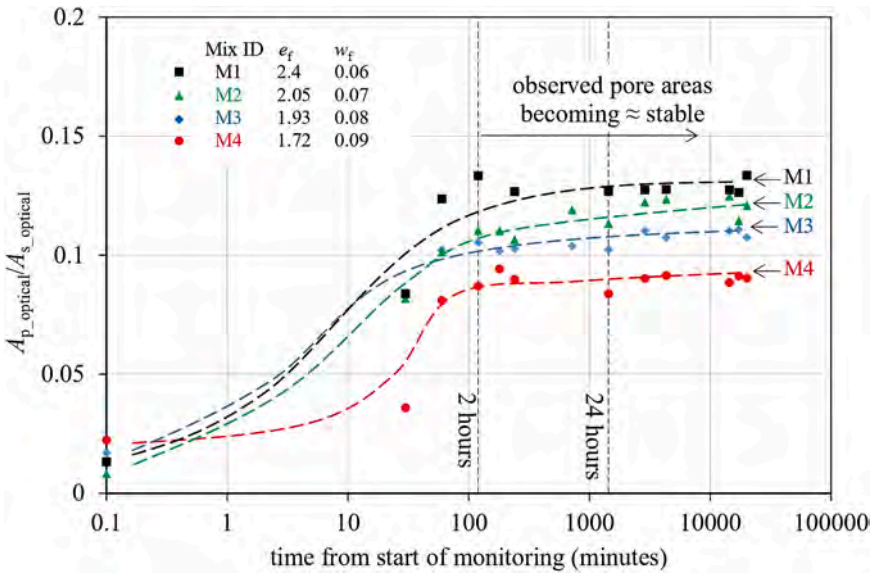

Fig. 12. ($A_{p\_optical}/A_{s\_optical}$) of hydrating samples obtained from digital imaging analysis.

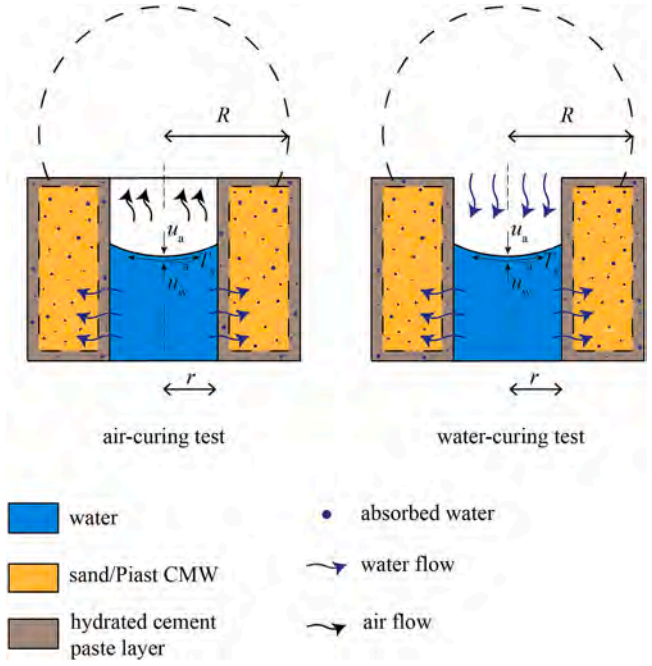

Fig. 13. Idealised capillary tube models for hydrating foam concrete samples.

where T_s, α, R, r are surface tension of the air-water interface, pore water-pore solid contact angle, radius of air-water interface curvature (known as water meniscus) and radius of the average pore, respectively. Eq. 4 demonstrates a dependency between s and the pore geometry idealised in Fig. 13. Also, s is dependent on degree of saturation $Sr=V_w/(V_a+V_w)$ where V_a, V_w are pore air and pore water volumes, respectively, as has been established previously, by many e.g., [48].

In both air-curing and water-curing test samples, the following processes are active at the pore scale:

- Process 1: the formation of hydration product(s) reduces the average pore diameter. Fig. 12 and visual observation in the laboratory indicate that the pore solid network becomes stable after approximately 2 h of hydration.
- Process 2: an amount of water is absorbed by the Piast CMW, and an amount of water is consumed in cement hydration, thus reducing the volume of pore water (V_w). Fig. 9 shows that more V_w continues to be absorbed into the samples containing higher percentages of CMW at the end of the monitoring period.

For water-curing test samples, another process is active at the pore scale:

- Process 3: an amount of water is supplied via the water burette (Fig. 6), thus V_w is increasing.

In air-curing tests, in the hours immediately after pouring, process 1 caused a decrease in r and R (Fig. 13) and process 2 caused a decrease in the degree of saturation Sr; together, they caused a rapid increase in the matric suction s. After process 1 has substantially subsided, process 2 remained active thus Sr kept decreasing and s kept increasing, the rate of which depended on the CMW content in the samples, i.e., slower rate of increase for samples with lower percentage of CMW (as is evident in Fig. 11). After a period of time, Sr reduced to residual values [48,49] and further removal of the water from the pores (by process 2 i.e., by being absorbed by the CMW and consumed in cement hydration) has led to very rapid increase in s (Fig. 11). The higher the mass percentage of Piast CMW was present in a foam concrete sample, the more water was removed from the pore spaces due to processes 1 and 2, which caused a higher matric suction s and a tightening/closing of the pore spaces, resulting in a higher ρ_{d_f}.

In water-curing tests after 1 to 4 h following pouring, process 3 was active in addition to processes 1 and 2 to dampen the increase in matric suction s. This is reflected in the overall lower magnitudes of the matric suction increase within the first 1–3 days in water-curing test samples compared to those in air-curing test samples (Fig. 10 compared to Fig. 11). Once process 1 had substantially stopped, processes 2 and 3 remained active, however process 2 gradually diminished (evident in the water-curing test results in Fig. 9) causing the matric suction s to slowly decrease over time (Fig. 10).

5. Conclusions

This paper reports on a novel laboratory set-up and experimental procedures designed to investigate the impact of different curing conditions on early age behaviour of foam concrete made with a CMW from

Piast mine in Poland, and the influence of the replacement of natural sand by the CMW. In summary, the following conclusions can be drawn:

- Custom-built unsaturated oedometer cells equipped with Warwick HCTs are the key to enable this investigation of hydrating foam concrete behaviour. Similar to Jamali et al. [32], HCTs were found to be capable of successfully measuring real time matric suction inside hydrating foam concrete samples, providing important data for interpreting physical processes feasibly active during their early age formation.
- This paper described how a foam-making device can be put together from standard laboratory equipment, how a protein-based foaming agent can be characterised to select a suitable dilution ratio and air pressure to generate stable foam for concrete-making, how digital imaging can be used to comprehend the visual observations and help interpreting the experimental data. The steps described are relatively simple and can be readily adapted to suit other investigations into properties of protein-based foam concrete materials.
- This study has confirmed previous data that curing plays an important role in governing the porosity of a hardened foam concrete [24, 27,50,51]. This was achieved by tracking the development of matric suction in hydrating foam concrete samples to show clearly that it evolves differently in response to different curing environments, and contributes to their eventual different properties.
- In this investigation, two different types of tests (both required approximately 14 days of monitoring) were devised for measuring the impacts of two different curing environments on foam concrete properties. The first type of test was adapted for a water-curing condition and is akin to a chemical shrinkage test. It was found from the first type of test that the volume of water consumed in cement hydration increased sharply with higher percentages of the CMW incorporated into the mix design; in correspondence, the matric suction increased to higher values in samples with lower percentages of the CMW.
- The second type of test was adapted for an air-curing condition where water inflow was not permitted into the hydrating foam concrete sample over the monitoring period. It was found that the increase in matric suction depends on the formation and stabilisation of the pore solid network as well as the gradual drying-out of the pore spaces due to pore water being consumed for concrete hydration and also absorbed by the fillers. In these air-curing tests, the matric suction, for the most part, was higher in samples with higher percentages of the CMW, causing the tightening and closing of some pore spaces which in turn resulted in their higher final dry densities.

CRediT authorship contribution statement

Esegbushota Josephine Foghi: Writing – original draft, Methodology, Investigation, Formal analysis, Data curation. **Thanh Vo:** Writing – original draft, Validation, Methodology, Investigation, Formal analysis, Conceptualization. **Mohammad Rezania:** Writing – review & editing, Validation, Supervision, Methodology, Investigation, Funding acquisition, Conceptualization. **Mohaddeseh Mousavi Nezhad:** Writing – review & editing, Supervision, Investigation, Funding acquisition. **Liberato Ferrara:** Writing – review & editing, Validation.

Declaration of Competing Interest

The authors declare that they have no known competing financial interests or personal relationships that could have appeared to influence the work reported in this paper.

Data Availability

Data will be made available on request.

Acknowledgment

The financial support of the RFCS project MINRESCUE (Contract RFCS-RPJ-899518) funded by the European Commission is gratefully acknowledged. Support by GIG Research Institute, Poland, in providing Piast CMW for experimentation is gratefully acknowledged. The first author also expresses appreciation to the financial support from The Niger Delta Development Commission, Nigeria.

References

[1] L. Haibin, L. Zhenling, Recycling utilization patterns of coal mining waste in China, Resour., Conserv. Recycl. vol. 56 (2014) 113–127.
[2] T.L. Vo, W. Nash, M. Del Galdo, M. Rezania, R. Crane, M.M. Nezhad, L. Ferrara, Coal mining wastes valorization as raw geomaterials in construction: a review with new perspectives, J. Clean. Prod. vol. 336 (2022).
[3] Z. Bian, J. Dong, S. Lei, The impact of disposal and treatment of coal mining wastes on environment and farmland, Environ. Geol. vol. 58 (2009) 625–634.
[4] GCCA, About Cement & Concrete, 2022. [Online]. Available: https://gccassociation.org/our-story-cement-and-concrete/. [Accessed 24 October 2022].
[5] G.L. Golewski, Assessing of water absorption on concrete composites containing fly ash up to 30% in regards to structures completely immersed in water, no. e02337, Case Stud. Constr. Mater. vol. 19 (2023). no. e02337.
[6] A. Torres, J. Brandt, K. Learand, J. Liu, A looming tragedy of the sand commons: increasing sand extraction, trade, and consumption pose global sustainability challenges, Science vol. 357 (6355) (2017) 970–971.
[7] M. Zhou, Y. Dou, Y. Zhang, Y. Zhang, B. Zhang, Effects of the variety and content of coal gangue coarse aggregate on the mechanical properties of concrete, Constr. Build. Mater. vol. 220 (2019) 386–395.
[8] X.W. Ma, J.H. Liu, C.J. Shi, A review on the use of LWA as an internal curing agent of high performance cement-based materials, Constr. Build. Mater. vol. 218 (2019) 385–393.
[9] Y. Zhu, Y. Zhu, A. Wang, D. Sun, K. Liu, P. Liu, Y. Chu, Valorization of calcined coal gangue as coarse aggregate in concrete, Cem. Concr. Compos. (121) (2021).
[10] M. Del Galdo, L. Albertini and L. Ferrara, Mechanical characterization of concrete with recycled aggregates from coal mining wastes, in *Proceedings of the 6th fib International Congress on Concrete Innovation for Sustainability, Oslo,* 2022.
[11] Z. Zhang, J.L. Provis, A. Reid, H. Wang, Geopolymer foam concrete: an emerging material for sustainable construction, Constr. Build. Mater. vol. 56 (2014) 113–127.
[12] Y.Mugahed Amran, N. Farzadnia, A.A. Abang Ali, Properties and applications of foamed concrete; a review, Constr. Build. Mater. vol. 101 (2015) 990–1005.
[13] K. Ramamurthy, E.K. Kunhanandan Nambiar, G. Indu Siva Ranjani, A classification of studies on properties of foam concrete, Cem. Concr. Compos. (31) (2009) 388–396.
[14] L. Ferrara, A. Caverzan, A. Peled, "Collapsible" lightweight aggregate concrete - part I: material concept and preliminary characterization under static loadings, Mater. Struct. vol. 49 (5) (2016) 1733–1745.
[15] L. Ferrara, A. Caverzan, L. Nahum, A. Peled, "Collapsible" lightweight aggregate concrete - part ii: characterization under static and dynamic loadings, Mater. Struct. vol. 49 (5) (2016) 1747–1760.
[16] G.L. Golewski, Combined effect of coal fly ash (CFA) and nanosilica (nS) on the strength parameters and microstructural properties of eco-friendly concrete, Energies vol. 16 (1) (2023) 452.
[17] T. Shams, G. Schober, D. Heinz, S. Seifert, Rice husk ash as a silica source for the production of autoclaved aerated concrete - a chance to save energy and primary resources, J. Build. Eng. vol. 57 (2022).
[18] O. Gencel, O.Y. Bayraktar, G. Kapla, O. Arslan, M. Nodehi, A. Benli, A. Gholampour, T. Ozbakkaloglu, Lightweight foam concrete containing expanded perlite and glass sand: physico-mechanical, durability, and insulation properties, Constr. Build. Mater. vol. 320 (2022).
[19] Y. Zhang, D. Chen, Y. Liang, Study on engineering properties of foam concrete containing waste seashell, Constr. Build. Mater. vol. 260 (2020).
[20] X.Y. Cong, S. Lu, Y. Yao, Z. Wang, Fabrication and characterization of self-ignition coal gangue autoclaved aerated concrete, Mater. Des. vol. 97 (2016) 155–162.
[21] O.H. Oren, A. Gholampour, O. Gencel, T. Ozbakkaloglu, Physical and mechanical properties of foam concretes containing granulated blast furnace slag as fine aggregate, Constr. Build. Mater. vol. 238 (2020).
[22] Y.-g Chen, L.-l Guan, S.-y Zhu, W.-j Chen, Foamed concrete containing fly ash: properties and application to backfilling, Constr. Build. Mater. vol. 273 (2021).
[23] N. Zhang, H. Sun, X. Liu, J. Zhang, Early-age characteristics of red mud-coal gangue cementitious material, J. Hazard. Mater. (2009) 927–932.
[24] B. Yao, G. Ren, J. Huang, X. Gao, Influence of self-ignition coal gangue on properties of foam concrete with steam curing, Case Stud. Constr. Mater. (2022).
[25] D. Falliano, D. De Domenico, G. Ricciardi, E. Gugliandolo, Experimental investigation on the compressive strength of foamed concrete: effect of curing conditions, cement type, foaming agent and dry density, Constr. Build. Mater. vol. 165 (2018) 735–749.
[26] S.K. Lim, C.S. Tan, X. Zhao, T.C. Ling, Strength and toughness of lightweight foamed concrete with different sand grading, KSCE J. Civ. Eng. vol. 19 (7) (2015) 2191–2197.

[27] J. Jiang, Z. Lu, Y. Niu, J. Li, Y. Zhang, Study on the preparation and properties of high-porosity foamed concretes based on ordinary Portland cement, Mater. Des. vol. 92 (2016) 949–959.
[28] D. Falliano, D. De Domenico, A. Sciarrone, G. Ricciardia, L. Restuccia, J. Tulliani, Fracture behavior of lightweight foamed concrete: the crucial role of curing conditions, Theor. Appl. Fract. Mech. vol. 103 (2019).
[29] B. Feneuil, P. Aimedieu, M. Scheel, J. Perrin, N. Roussel, Stability criterion for fresh cement foams, Cem. Concr. Res. vol. 125 (2019).
[30] K. Dhasindrakrishna, K. Pasupathy, S. Ramakrishnan, J. Sanjayan, Effect of yield stress development on the foam-stability of aerated geopolymber concrete, Cem. Concr. Res. (2020).
[31] S. Cho, A. van Rooyen, E. Kears, G. van Zijl, Foam stability of 3D printable foamed concrete, J. Build. Eng. (2022).
[32] A. Jamali, J. Mendes, B. Nagaratnam, M. Lim, A new four stage model of capillary pressure in early age concrete: insights from high capacity tensiometers, Cem. Concr. Res. vol. 161 (2022).
[33] M. Bagheri, M. Rezania, M.M. Nezhad, Cavitation in high-capacity tensiometers: effect of water reservoir surface roughness, Geotech. Res. vol. 5 (2) (2018) 81–95.
[34] M. Bagheri, M.M. Nezhad, M. Rezania, A CRS oedometer cell for unsaturated and non-isothermal tests, Geotech. Test. J. vol. 43 (1) (2019) 20–37.
[35] A. Kashani, T.D. Ngo, A. Hajimohammadi, Effect of recycled glass fines on mechanical and durability properties of concrete foam in comparison with traditional cementitious fines, Cem. Concr. Compos. vol. 99 (2019) 120–129.
[36] Q.S. Khan, M.Neaz Sheikhb, T.J. McCarthy, M. Robati, M. Allen, Experimental investigation on foam concrete without and with recycled glass powder: a sustainable solution for future construction, Constr. Build. Mater. vol. 201 (2019) 369–379.
[37] BS ISO 20290–1, Aggregates for concrete - Test methods for mechanical and physical properties, British Standards Institution, 2021.
[38] E.K. Kunhanandan Nambiar, K. Ramamurthy, Air-void characterisation of foam concrete, Cem. Concr. Res. vol. 37 (2007) 221–230.
[39] A. Raj, D. Sathyan, K.M. Mini, Physical and functional characteristics of foam concrete: a review, Constr. Build. Mater. vol. 221 (2019) 787–799.
[40] T. Adams, A. Vollpracht, J. Haufe, L. Hildebrand, S. Brell-Cokcan, Ultra-lightweight foamed concrete for an automated facade application, Mag. Concr. Res. vol. 71 (8) (2019) 424–436.
[41] M. Bagheri, M. Rezania, M.M. Nezhad, Rate dependency and stress relaxation of unsaturated clays, Int. J. Geomech. vol. 19 (12) (2019) 04019128.
[42] M. Bagheri, M. Rezania, Effect of soil moisture evaporation rate on dynamic measurement of water retention curve with high-capacity tensiometer, p. 04021301, Int. J. Geomech. vol. 22 (3) (2022), p. 04021301.
[43] ASTM C1608, Standard Test Method for Chemical Shrinkage of Hydraulic Cement Paste C1608, American Standard for Testing Methods, New York, 2017.
[44] Z.-W. Liu, K. Zhao, Y.-f Tang, C. Hu, , Preparation of cenosphere microcapsules and their application in foam concrete, Mag. Concr. Res. vol. 72 (20) (2020) 1072–1080.
[45] Y. Song, D. Lange, Influence of fine inclusions on the morphology and mechanical performance of lightweight foam concrete, Cem. Concr. Compos. vol. 124 (2021).
[46] S.-Y. Chung, M.A. Elrahman, J.-S. Kim, T.-S. Han, D. Stephan, P. Sikora, Comparison of lightweight aggregate and foamed concrete with the same density level using image-based characterizations, Constr. Build. Mater. vol. 211 (2019) 988–999.
[47] M. Bouasker, P. Mounanga, P. Turcry, A. Loukili, A. Khelidj, Chemical shrinkage of cement pastes and mortars at very early age: effect of limestone filler and granular inclusions, Cem. Concr. Compos. vol. 30 (2008) 13–22.
[48] E. Buckingham, Studies on the movement of soil moisture, Washington, 1907.
[49] W.B. Haines, Studies in the physical properties of soil: v. the hysteresis effect in capillary properties and the modes of moisture distribution associated therewith, J. Agric. Sci. vol. 20 (1) (1930) 97–116.
[50] J. Bear. Hydraulics of Groundwater, 2nd ed., McGraw-Hill, New York, 1979.
[51] S. Wei, Z. Yunsheng, M. Jones, Using the ultrasonic wave transmission method to study the setting behavior of foamed concrete, Constr. Build. Mater. vol. 51 (2014) 62–74.